Scientific Research Publishing

Journal of Minerals and Materials Characterization and Engineering, 2023, 11, 131-142
https://www.scirp.org/journal/jmmce
ISSN Online: 2327-4085
ISSN Print: 2327-4077

Carbides Formation in MarM247 Directional Solidified during Stress-Rupture Test at High Temperature

Daniel Moreno*, Itzik Mizrahi, Yuri Lipkin, Vasiliy Zevin, Elinor Itzhak, Zion Harush

Beth Shemesh Engines Ltd., FAA & EASA, Beth Shemesh, Israel
Email: *danielm@bsel.co.il, Itzik.Mizrahi@bsel.co.il, Yuri.Lipkin@bsel.co.il, Vasiliy.Zevin@bsel.co.il, Elinor.Itzhak@bsel.co.il, nzionh@bsel.co.il

How to cite this paper: Moreno, D., Mizrahi, I., Lipkin, Y., Zevin, V., Itzhak, E. and Harush, Z. (2023) Carbides Formation in MarM247 Directional Solidified during Stress-Rupture Test at High Temperature. *Journal of Minerals and Materials Characterization and Engineering*, **11**, 131-142.
https://doi.org/10.4236/jmmce.2023.115011

Received: June 14, 2023
Accepted: September 5, 2023
Published: September 8, 2023

Abstract

In our study, stress-rupture tests were conducted at elevated temperatures to examine the impact of high temperature on MarM247 LC (low carbon). Our main objective was to investigate the alterations in the microstructure, particularly the carbon precipitation, during long-term stress-rupture tests. It was observed that cracks developed near the sample neck, following the path of the carbides and the gamma matrix, rather than occurring in the gamma-gamma prime eutectic. This occurred despite the formation of carbides because of prolonged exposure to high temperature and load, and the crack propagation did not follow that path. Based on these findings, we suggest that a reduction in the carbon content of Mar-M247 LC can enhance the sample's lifespan when subjected to temperatures below 760˚C and a stress of 690 MPa.

Keywords

MarM247, Carbides, Stress-Rupture, High-Temperature, Crack-Propagation

1. Introduction

The demand for high-performance alloys in the manufacturing of turbine blades for fuel-efficient aircraft engines has led to the advancement of production technologies and the development of nickel-based superalloys [1] [2] [3] [4]. One of the main causes of failure in polycrystalline blades under high load and temperature is the presence of perpendicular or nearly perpendicular grain boundaries to the applied mechanical stress, which are weak points in the material. Over time, these failure sources, subjected to alternating stresses and high temperatures, degrade the metallurgical state of the alloy. To address this issue, Directional Solidification (DS) and Single Crystal (SC) casting technologies have been developed, enabling the production of superalloy blades without grain boundaries perpendicular to the load in DS or without grains altogether in the case of SC. These advancements have improved the service life and performance of the engine [5] [6]. Furthermore, to optimize the alloying elements and enhance efficiency in the engines, these new casting technologies were integrated with conventional cast equiaxed alloys that were already available [5] [6].

The casting process of Mar-M247 alloy, which encompasses the solidification temperature range of 1172˚C to 1187˚C, involves constitutional decomposition in the as-cast product, resulting in small eutectic compositions of gamma and gamma prime in the inter-dendritic zones [7]. The processing of nickel-based superalloys includes heat treatment, which entails the dissolution of the "butterfly-shaped" gamma prime phase formed during the cooling of the cast product. This is followed by rapid cooling to achieve small-sized spherical gamma prime phases, and ultimately, aging to obtain an optimal cuboidal gamma prime structure with high density in the gamma matrix. The eutectic compositions of gamma and gamma prime in the inter-dendritic regions are highly sensitive to incipient melting during the solution heat treatment and are crucial for the final mechanical properties of the superalloy at high temperatures. However, the formation of undesirable phases such as carbides, topologically close-packed (TCP) phases (sigma, μ, and Laves phases), also affects the mechanical properties of the alloys [8].

In Mar-M247 alloy, an additional amount of Nb was introduced to modify the ideal conditions for solution heat treatment. The recommended temperature for this treatment is approximately 1260˚C for 8 hours, which enables the alloy to achieve a homogeneous gamma matrix with fine gamma prime phases. However, incipient melting was observed at 1280˚C in this alloy [9]. Thermodynamic calculations have shown that the lower temperature for solutioning in Mar-M247 superalloy is around 1220˚C. At 1210˚C, eutectic microstructures were observed in the inter-dendritic regions after a long period of heat treatment [10].

The instability of microstructures in superalloys was investigated after creep tests at high temperatures to evaluate their impact on mechanical properties. It was found that the nucleation of microcracks primarily occurs in high-angle boundaries inclined to the stress axis [11]. However, changes in certain metallurgical microstructures showed low correlation with the failure process. Electromagnetic techniques were employed to estimate the remaining lifespan of a nickel-based alloy under low-cycle fatigue, considering the effect of chromium depletion on the paramagnetic and ferromagnetic properties of the alloy [12]. The chromium content at the crack surfaces increased, and oxygen was detected on the surface and crack flanks. Kirka *et al.* reported that the aged microstructure of directionally solidified Ni-based superalloys does not significantly affect fatigue life, except in the case of perpendicular rafted microstructures, which led to an increase in the number of cycles until failure occurred [13]. In a high-resolution transmission electron microscopy (HRTEM) study conducted by Smith *et al.* [14], it was observed that the χ and η phases, along with the γ′ stacking faults, exhibit a strong correlation with improved creep strength. The use of advanced techniques and chemical mapping allowed for the identification of specific lattice sites where elemental segregation occurs in conjunction with lattice faults. Atomistic studies focused on controlling deformation at the atomic level revealed that Nb and Ta are promising alloying elements for inducing transformations in the χ and η phases, whereas Re, W, and Mo show promise in Co alloys [14].

Furthermore, it was reported [15] that carbide growth occurs during high-temperature exposure in creep tests. In many instances, the presence of carbides enhances the resistance of superalloys to high temperatures under moderate loads. However, in some cases, the development of carbides within microporosity sites can lead to the initiation of micro-cracks, eventually resulting in failure.

The main objective of this research is to examine the alterations and failure mechanisms that arise in MarM247 LC (low carbon) following stress-rupture tests conducted at high temperatures. The investigation focuses on the metamorphosis of the metallurgical structure and aims to identify the source of the final failure.

2. Experimental

A commercial MarM247LC superalloy ingot, with a chemical composition summarized in **Table 1**, was cast using a directional solidification process in an ALD single crystal furnace. This process yielded 15 directional solidified rods, each measuring 15 mm in diameter and 210 mm in length. Metallographic inspection revealed the presence of 3 to 6 grains in the cross-section, with a unified growth direction predominantly near the <001> orientation as the preferred growth direction for this superalloy. Following inspection, the rods were subjected to a full standard heat treatment.

After undergoing a solutioning treatment at 1250˚C for 2 hours, the rods were subjected to a two-stage aging process for precipitation treatment. The first stage involved aging at 1079˚C for 4 hours, followed by a second stage aging at 871˚C for 20 hours, with subsequent cooling in argon gas. The temperature accuracy within the furnace was maintained within ±2˚C, and the entire heat treatment

Table 1. Chemical composition of Mar-M247LC used in the presented work.

Elements (Ni bal.)	Co	Cr	Al	Ta	W	Ti	Mo	Hf	B	Zr	C
Standard (wt./o)	9 - 9.5	8 - 8.5	5.4 - 5.7	3.1 - 3.3	9.3 - 9.7	0.6 - 0.9	0.4 - 0.6	1.4 - 1.6	0.01 - 0.02	0.007 - 0.02	0.07 - 0.08
This work (wt./o)	9.17	8.38	5.68	3.21	9.44	0.76	0.53	1.54	0.016	0.012	0.078

Traces elements and boiling point elements according to standard AMS2280.

process was conducted under a vacuum of 10^{-4} mbar.

Following the heat treatment, the rods were machined into bond-shaped samples, with a 1/2-inch screw (NCX13) adapted to the stress-rupture test grips. The samples featured a graded reduction from the 12 mm diameter to a 6.35 mm diameter along the 37 mm gauge length of the sample obtaining 6 mm radius in a graded reduction. The total length of the sample was 86 mm. Tensile tests were conducted on these samples at 760˚C to assess their mechanical properties. The master alloy, tested prior to compliance, exhibited favorable results with a yield strength (0.2% offset) of 907 MPa, ultimate tensile strength (UTS) of 1093 MPa, and 14% elongation in 4D.

The machined directional solidified rods were then subjected to stress rupture tests at different temperatures and stress levels. Specifically, the tests were conducted at 690 MPa, 221 MPa, and 138 MPa, at temperatures of 760˚C, 982˚C, and 1038˚C, respectively. Upon failure, the remaining portions of the samples were cross-sectioned, with particular focus on the region near the neck where the maximum deformation occurred. This allowed for the observation of microstructural changes under load and prolonged exposure to high temperatures.

This work specifically reports on the post-stress rupture metallographic cross-section of the sample that endured 711 hours under a stress of 690 MPa at 760˚C. The aim is to investigate the microstructural changes along different regions of the samples exposed to varying loads, including the screw zone (experiencing very low stresses), the graded reduction diameter zone between the screw zone and the gauge length (experiencing moderate stresses), the gauge length (experiencing high stresses), and the region near the neck (experiencing the maximum deformation). The microstructure was examined using optical microscopy and SEM-EDS techniques.

3. Results

In Table 2 and Table 3 the mechanical properties of the samples are reported:

Table 2. Stress-Strain test.

Temperature [˚C]	Y.P (0.2%)	UTS [MPa]	D_o Start Dia. [mm]	D_f Final Dia. [mm]	Reduction Area [%]
870˚C	766	938	6.350	5.889	14

Table 3. Stress-Rupture test.

Temperature [˚C]	Stress [MPa]	D_o Start Dia. [mm]	D_f Final Dia. [mm]	Reduction Area [%]	Lifetime [hours]	Over Lifetime factor from Standards
760	690	6.35	5.627	21.5	711	3.57
980	221	6.36	4.19	56.7	68.5	1.37
1040	138	6.35	3.64	67.1	158	2.63

In this study, the focus was targeted to the cross sections of the mechanical properties sample that achieve 711 hr. under 690 MPa at 760˚C, presented according to **Figure 1**, in **Figures 2-4**. Zones B and C present an unaffected structure by the load applied rather than zones D and E that present some nucleation of carbides and nitrides that show to be the sources of the discontinuities and inter-dendritic micro-cracks. The carbides and nitrides phases exist in all the zones in the sample even in the pre-load sample as show **Figure 3(A)**, but **Figure 3(E)** zone present some evidence of carbides conglomeration under load, high temperature and time that can be source to the weakness of the E zone and the micro-cracks formation in the carbide traces path. In the other hand, the crack propagation avoids the gamma-gamma prime eutectic as shows **Figure 4**.

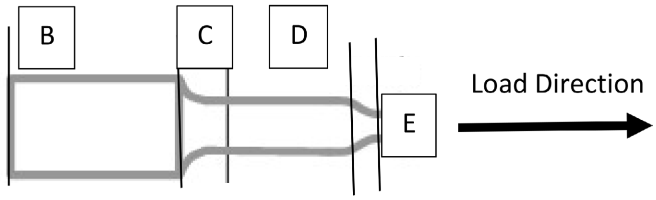

Figure 1. Screw (B), graded reduction diameter (C), gauge length (D), and neck (E) zones metallurgical characterized in follow figures. (A) is referred to the heat-treated structure before loading (no in the scheme).

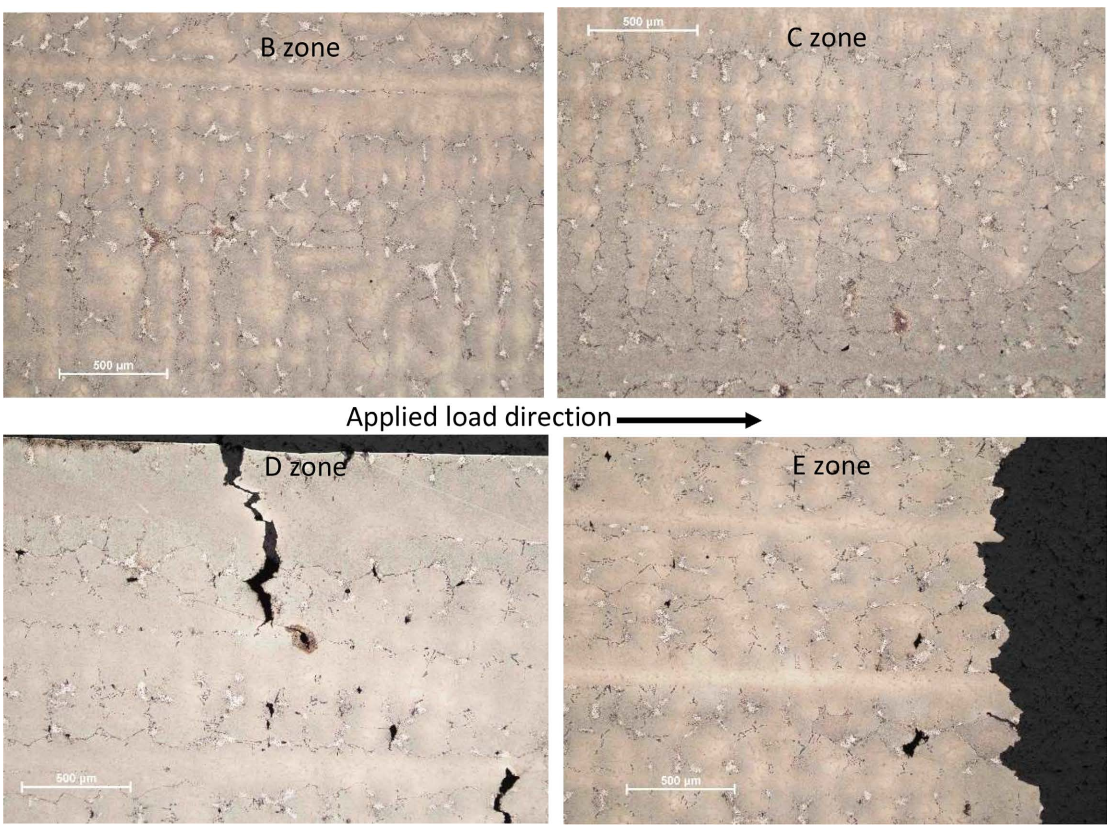

Figure 2. Dendrite microstructure under optical microscope of the four zones of the sample. Micro-discontinuities as crack sources propagation were observed in the gauge length (D) and neck (E) zones. No differences were found between the pre-loaded A zone, B zone and C zone.

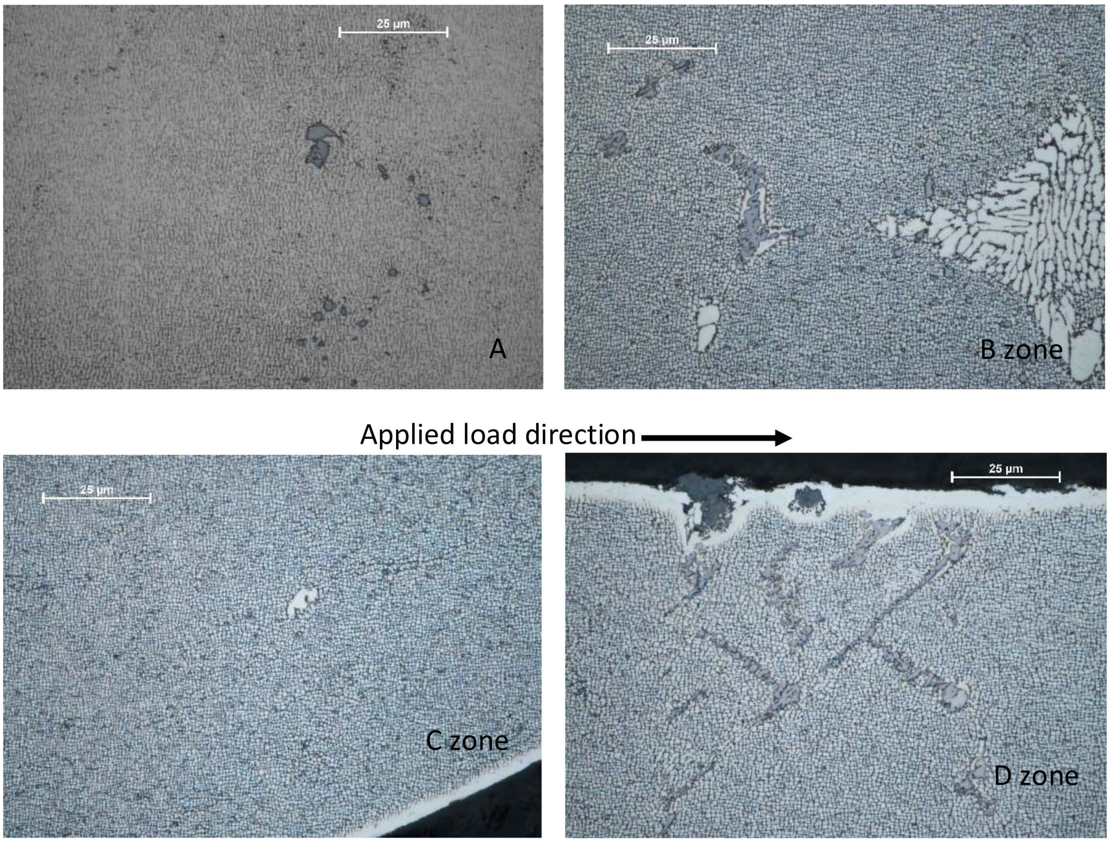

Figure 3. Higher magnification under optical microscope of the sample before loading (A) and the 690 MPa loading at 760˚C during 711 hr. sample zones of the sample. Long exposure to the sample conditions in the rupture stress test do not show rafting but a small refining of the precipitates.

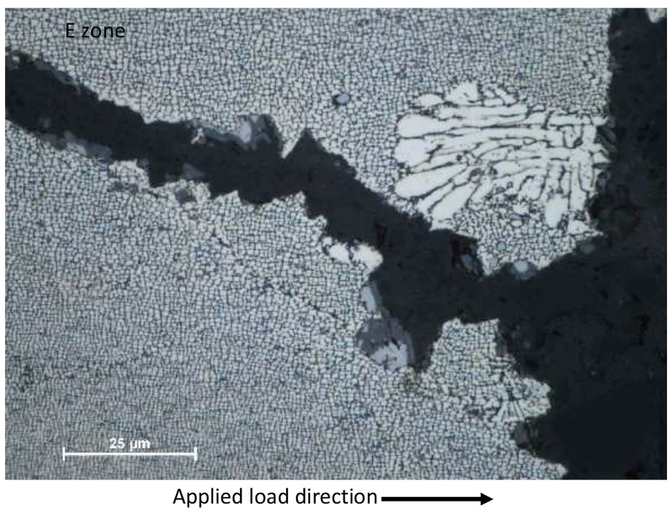

Figure 4. Higher optical microscope magnification of the neck crack propagation zone (E zone) under the 690 MPa loading at 760˚C during 711 hr. MC and NC phases can be observed in the crack propagation path. The gamma-gamma prime eutectic phase is not in the path.

Scanning electron microscopy (SEM) and electron diffraction spectroscopy (EDS) in **Figures 5-7** reveled the present of new phase elaborated during the long-term test under 690 MPa loading at 760˚C during 711 hr. but no precipitation coarsening or rafting.

Figure 5 shows the precipitates along the sample in the different zones without significant change of the precipitates compared to A that represent the metallography micro-structure of the sample after heat treatment. Figure 6 compare two gamma-gamma prime eutectic structures' one in the neck (zone E) and in the screw (zone B). The formation of carbides under high load at high temperature can be observed in the right image in Figure 6 that represent a nearest gamma-gamma prime eutectic to the crack path. In the other hand, the left

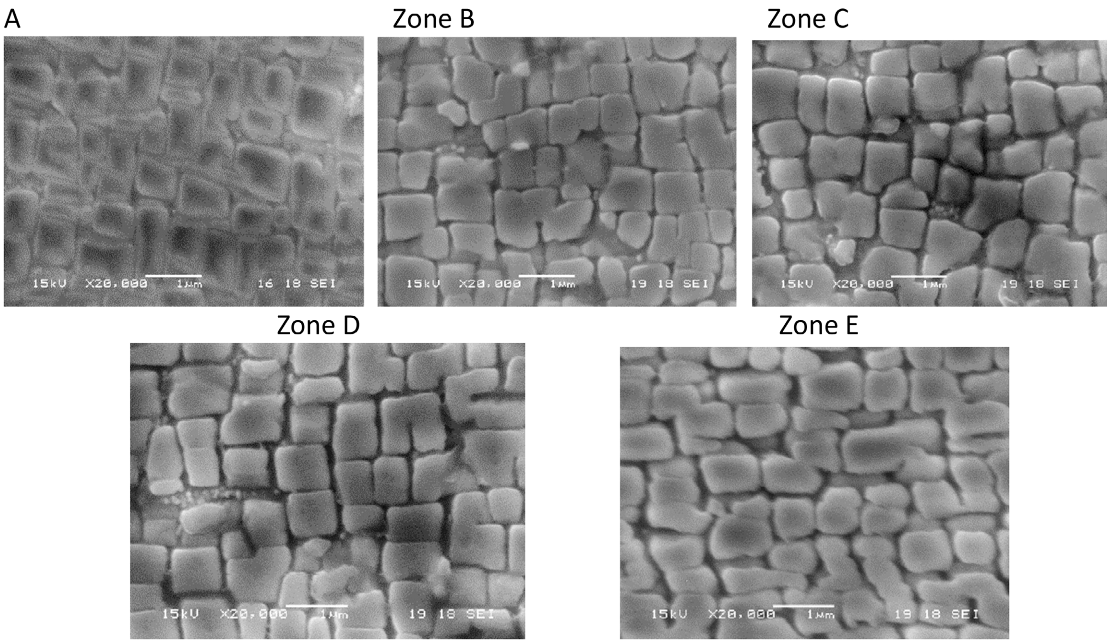

Figure 5. SEM images and comparison between gamma prime precipitates in A after heat treatment only and different zones of the sample according to Figure 1 after stress rupture test under 690 MPa at 760˚C during 711 hr. No significant changes can be observed in the precipitate structures.

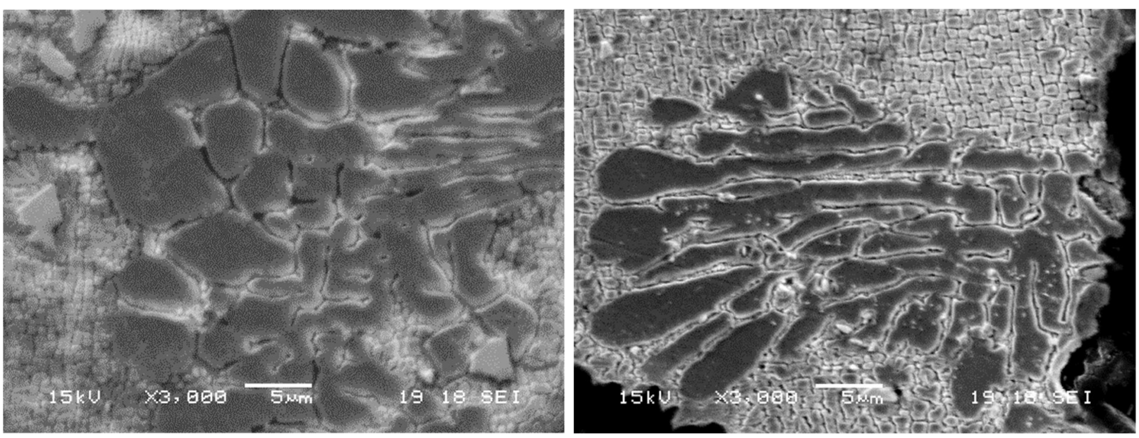

Figure 6. SEM images and comparison between gamma-gamma prime eutectic in zone B (screw zone) where no load affects the micro-structure (5 zone B - left), and gamma-gamma prime phase near the crack propagation zone (E zone - right) under the 690 MPa loading at 760˚C during 711 hr. where the development and increasing of MC phases can be observed in the crack propagation path (Figure 4) and inside the gamma-gamma prime eutectic.

Table 4. EDS chemical analysis of the carbides in the image of Figure 7 according to the marked points on the picture.

Elements	C	N	Cr	Ni	Ta	W
			Weight %			
Point 1	7.81	0	7.25	71.23	13.71	0.00
Point 2	7.30	0	3.34	77.64	0.00	11.71
Point 3	5.51	0	8.46	72.14	0.00	13.88
Point 4	4.34	0	7.19	64.17	9.77	14.53
Point 5	5.62	0	12.65	67.65	3.19	10.89
Point 6	6.17	0	6.39	64.37	12.30	10.77
			Weight % error (±1 Sigma)			
Point 1	±0.34	0	±0.78	±5.44	±9.56	0.00
Point 2	±0.29	0	±0.55	±4.52	0.00	±0.83
Point 3	±0.29	0	±1.28	±4.80	0.00	±0.91
Point 4	±0.24	0	±1.07	±4.17	±6.56	±2.49
Point 5	±0.25	0	±1.20	±3.01	±5.62	±0.74
Point 6	±0.24	0	±0.53	±2.70	±5.37	±0.70
			Atom %			
Point 1	31.28	0	6.71	58.37	3.65	0.00
Point 2	29.54	0	3.12	64.24	0.00	3.10
Point 3	23.82	0	8.45	63.80	0.00	3.92
Point 4	20.93	0	8.02	63.34	3.13	4.58
Point 5	24.13	0	12.53	59.38	0.91	3.05
Point 6	27.63	0	6.60	58.96	3.66	3.15

image in Figure 6 represent a gamma-gamma prime eutectic in the screw where no load but same temperature of the sample insignificant number of carbides can be observed.

EDS analysis was carried out on the sample shown in the right image of Figure 6 as can be seen in Figure 7. Six points of the new phases to be suspected as carbides in the picture were analyzed, and the results summarized in Table 4. Elements that form carbide as Cr, Ta and W were detected with a parallel amount of carbon in all points. No nitrogenized phases were found.

4. Discussion

The main purpose of this study is to investigate the changes in microstructure during the exposure of a directional solidified Mar-M247 LC sample to a stress of 690 MPa at 760˚C for 711 hours. The microstructure observations did not reveal significant precipitation changes in the gamma prime phase or rafting, but

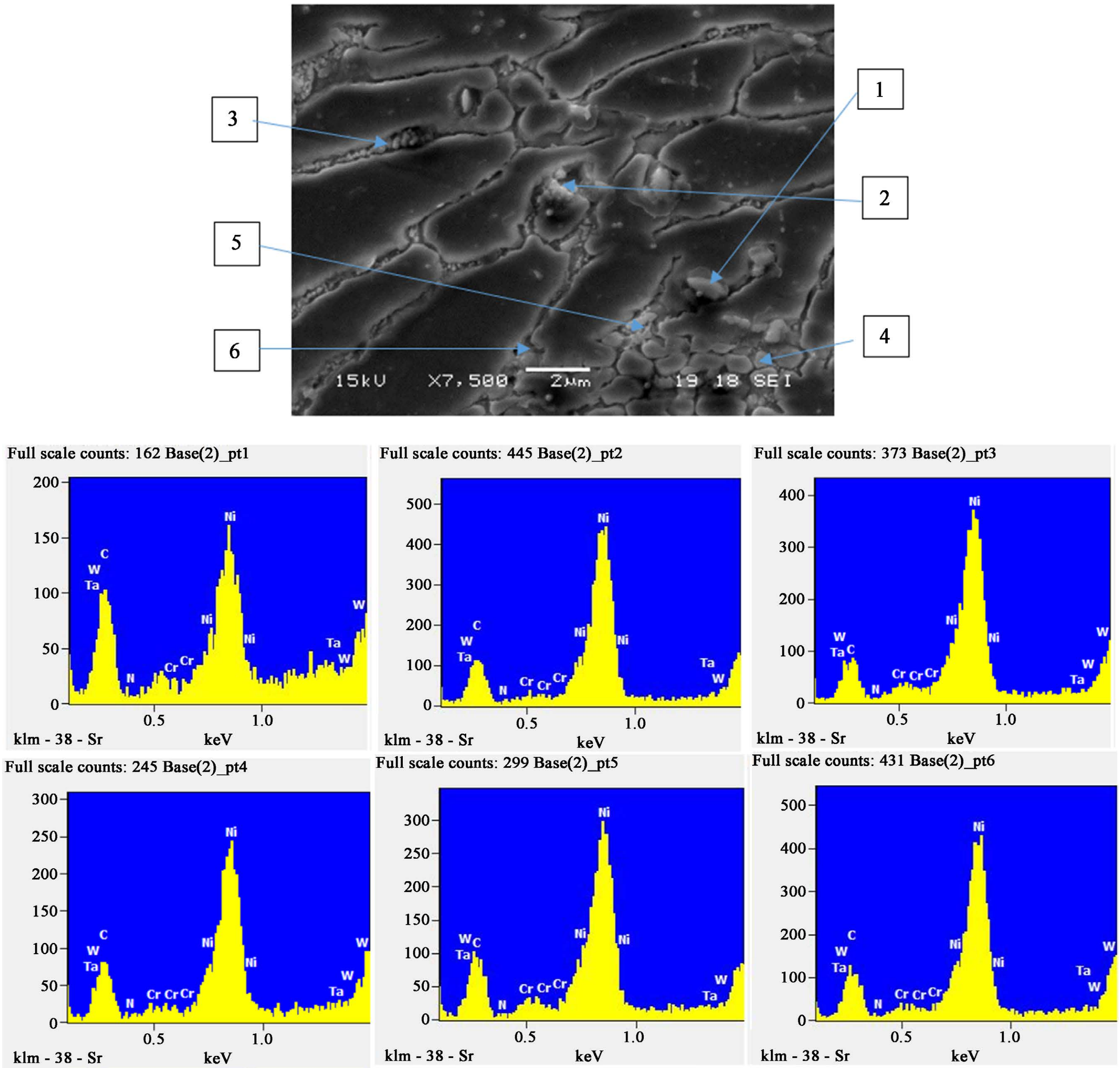

Figure 7. The gamma-gamma prime eutectic area near the crack path and the EDS chemical analysis carried out in the suspected carbides phases points. Chemical values are summarized in Table 4.

there was an increase in the presence of carbides. The aggregation of these carbides within the gamma matrix could potentially be related to the formation of microcracks under the combined influence of load and temperature.

Previous research conducted by Li *et al.* [16] concluded that at 850˚C, the secondary gamma prime phase did not exhibit significant growth, whereas the tertiary gamma prime phase clearly coarsened. However, we did not observe this behavior at 760˚C in our study. Li also noted that Ta forms a gamma prime film around MC and $M_{23}C_6$ carbide types, leading to a decrease in mechanical properties during thermal exposure [16]. Kalyanasundaram *et al.* [17] further emphasized this behavior by presenting scanning electron microscopy images showing coarsening carbides, which were attributed to thermal exposure and shear stresses. These carbides were found to agglomerate near cracks, while gamma prime was located close to the fracture in samples exposed to stresses ranging from 500 - 650 MPa at 800˚C.

Figure 3 illustrates zone D, where coarsening carbide agglomeration is observed, resembling a shear band in FCC alloys within a <01-1> {111} crystallographic shear system, as reported elsewhere [18]. These findings strongly suggest that the driving force behind carbide formation is associated with shear bands, but further investigation using different techniques is needed to confirm this. Recently, Nordin *et al.* [19] used the Differential Scanning Calorimetric (DSC) technic to characterize the crystallization kinetic of a high entropy bulk samples and the average activation energy value. The DSC technic could be used to confirm the process and formation kinetics of the carbide formation presented in this paper as a future study. **Figure 4** shows the sample fouler crack and emphasize the conglomeration of suspected carbides all the crack path. Moreover, in the gamma gamma-prime eutectic near the crack path many suspected carbides can be observed that sustain the assumption that carbides are formed during the long-term stress rupture test and the sample weakness in the neck zone is attributed to the brittleness of those phases, correspond to M_xC_y compositions. The detection of high amount of major elements that crate carbides as Cr, Ta, W, with high correlation with the Carbon amount presented in **Figure 6** & **Figure 7** and **Table 4**, support the assumption that these small particle phases are carbides.

5. Conclusions

The main conclusions in the present work can be summarized as follows:

1) During the stress rupture test at temperatures lower than 760˚C, no gamma-prime coarsening or rafting was observed after 711 hours under 690 MPa.

2) In the neck (zone E) under the same conditions, but in addition of maximum deformation, precipitation of carbides was observed.

3) No carbide precipitation was found at 760˚C during 711 hours without load.

4) Cracks were found near the sample neck that followed the path of the carbides and the gamma matrix in addition to the gamma-gamma prime eutectic outside boundaries, despite the formation of carbides in the eutectic phase.

5) Based on our findings; we can suggest that by reducing carbon amount in Mar-M247 LC can improve the lifetime of the sample at temperatures lower than 760˚C under stresses.

Conflicts of Interest

The authors declare no conflicts of interest regarding the publication of this paper.

References

[1] Strangman, T.E. and Hoppin III, G.S. (1980) Development of Exothermically Cast

Single Crystal MarM247 and Derivative Alloys. *Proceedings of the 4th International Symposium on Superalloys*, Champion, 21-25 September 1980, 215-224. https://doi.org/10.7449/1980/Superalloys_1980_215_224

[2] Hoppin III, G.S., Fujii, M. and Strangman, T.E. (1977) Low-Cost Single-Crystal Turbine Blades. NASA-Lewis Research Center Contract NAS 3.20073, July 1977-December 1979.

[3] Duhl, D.N. and Nguyen-Dmh, X. (1980) Evaluation of Single Crystal Superalloys. *AIME Annual Meeting*, Las Vegas, 24-28 February 1980, 215-224.

[4] Strangman, T.E., Fujii, M. and Nguyen-Dinh, X. (1980) Development of Coated Single Crystal Superalloy System for Gas Turbine Applications. *Proceedings of the 4th International Symposium on Superalloys*, Champion, 21-25 September 1980, 795-804.

[5] Harris, K., Erickson, G.L. and Schwe, R.E. (1984) MAR-M247 Derivations—CM 247 LC DS Alloy CMSX Single Crystal Alloy Properties and Performance. *Superalloy 1984 Conference Proceeding*, Champion, 7-11 October 1984, 221-230.

[6] Harris, K. and Erickson, G.L. (1979) Vacuum Induction Refined MM 0011 (MAR M-247) for Investment Cast Turbine Components. *Proceedings of 6th International Vacuum Metallurgy Conference on Special Melting*, San Diego, 23-27 April 1979, 319-339.

[7] Przeliorz, R. and Piątkowski, J. (2017) Application of DSC Method in Studies on Phase Transitions of Ni Superalloys. *Archives of Foundry Engineering*, **17**, 133-136. https://doi.org/10.1515/afe-2017-0144

[8] Luo, W., Xie, Z.C., Zhang, S.Y., *et al.* (2023) Tailoring the Plasticity of Topologically Close-Packed Phases via the Crystals' Fundamental Building Blocks. *Advanced Materials*, **2023**, Article ID: 2300586. https://doi.org/10.1002/adma.202300586

[9] Azevedo e Silva, P.R.S., Baldan, R., Nunes, C.A., Coelho, G.C. and da Silva Costa, A.M. (2013) Solution Heat-Treatment of Nb-Modified MAR-M247 Superalloy. *Material Characterization*, **75**, 214-219.

[10] Baldan, R., da Rocha, R.L.P., Tomasiello, R.B., *et al.* (2013) Solutioning and Aging of MAR-M247 Nickel-Based Superalloy. *Journal of Materials Engineering and Performance*, **22**, 2574-2579. https://doi.org/10.1007/s11665-013-0565-4

[11] Lavigne, O., Ramusat, C., Drawin, S., Caron, P., Boivin, D. and Pouchou, J.-L. (2004) Relationships between Microstructural and Mechanical Properties Behavior in New Generation Nickel-Base Single Crystal Superalloys. *Superalloys* 2004: *Proceedings of the 10th International Symposium on Superalloys*, Champion, 19-23 September 2004, 667-675. https://www.tms.org/Superalloys/10.7449/2004/Superalloys_2004_667_675.pdf

[12] Barton, S., Weiss, M.K.-B. and Maier, H.J. (2022) *In-Situ* Characterization of Microstructural Changes in Alloy 718 during High-Temperature Low-Cycle Fatigue. *Metals*, **12**, Article No. 1871. https://doi.org/10.3390/met12111871

[13] Kirka, M.M., Brindley, K.A., Neu, R.W., Antolovich, S.D., Shinde, S.R. and Gravett, P.W. (2015) Influence of Coarsened and Rafted Microstructures on the Thermomechanical Fatigue of a Ni-Base Superalloy. *International Journal of Fatigue*, **81**, 191-201. https://doi.org/10.1016/j.ijfatigue.2015.08.001

[14] Smith, T.M., Zarkevich, N.A., Egan, A.J., *et al.* (2021) Utilizing Local Phase Transformation Strengthening for Nickel-Base Superalloys. *Communications Materials*, **2**, Article No. 106. https://doi.org/10.1038/s43246-021-00210-6

[15] Liu, L.R., Jin, T., Zhao, N.R., Sun, X.F., Guan, H.R. and Hu, Z.Q. (2003) Formation of Carbides and Their Effects on Stress Rupture of a Ni-Base Single Crystal Supe-

ralloy. *Materials Science and Engineering A*, **361**, 191-197.
https://doi.org/10.1016/S0921-5093(03)00517-3

[16] Li, L.X., Gong, X.F., Wang, C.S., Wu, Y.S., Yu, H.Y., Su, H.J. and Zhou, L.Z. (2021) Correlation between Phase Stability and Tensile Properties of the Ni-Based Superalloy MAR-M247. *Acta Metallurgica Sinica* (*English Letters*), **34**, 872-884.
https://www.amse.org.cn/EN/10.1007/s40195-020-01139-4

[17] Kalyanasundarama, V., De Lucaa, A., Wróbel, R., Tanga, J., Holdswortha, S.R., Leinenbacha, C. and Hosseini, E. (2023) Tensile and Creep-Rupture Response of Additively Manufactured Nickel-Based Superalloy CM247LC. *Additive Manufacturing Letters*, **5**, Article ID: 100119. https://doi.org/10.1016/j.addlet.2022.100119

[18] Eggeler, G., Wieczorek, N., Fox, F., Berglund, S., Burger, D., Dlouhy, A., *et al.* (2018) On Shear Testing of Single Crystal Ni-Base Superalloys. *Metallurgical and Materials Transactions A*, **49**, 3951-3962.
https://doi.org/10.1007/s11661-018-4726-9

[19] Nordin, N.H., Mohamad, F.S. and Jamal, N.A. (2020) Non-Isothermal Crystallization Kinetics of a Rapidly Solidified as-Cast TiZrHfNiCu High Entropy Bulk Metallic Glass. *World Journal of Engineering and Technology*, **8**, 280-295.
https://doi.org/10.4236/wjet.2020.83023